On the Effectiveness Factor of Flow-Through Porous Electrodes

Mahmoud M. Saleh*

Chemistry Department, Faculty of Science, Cairo University, Egypt

Received: April 6, 2004; In Final Form: June 13, 2004

An effectiveness factor, Φ, was introduced to investigate the effects of different parameters on the utilization extent of a flow-through porous electrode operating for simultaneous reactions. A mathematical model helped to study the effects of ohmic resistance, mass transfer, kinetics, and bubble formation on the effectiveness factor for the main reaction (metal deposition taken as an example). This was presented as a set of dimensional and dimensionless groups. These groups are the following: total theoretical limiting current, I_L; conductivity group, σ; kinetic ratio, I_o; and the bubble group, Ψ. The results showed that Φ increases at higher σ, lower I_L and I_o, and higher Ψ (high Ψ means lower extents of bubble formation). The ohmic resistance pushed the reaction to a small layer at the front of the electrode, resulting in a situation in which the reaction is limited at the front of the electrode (higher polarizations) but operates at lower currents at the back of the electrode (lower polarizations). Improvement of Φ values at higher I_L and/or I_o (i.e., at higher rates) could be obtained by using higher values of σ. Because σ depends on structure, transport, and kinetic parameters, it could help to guide the design of the porous electrode. A simultaneous side reaction (hydrogen evolution reaction, HER) retarded operating the cell at higher currents and confined estimation of the limiting currents of the main reaction. The bubble formation accentuates the ohmic effects. A satisfactory agreement between the model predictions and the experimental data was obtained.

Introduction

It is optimal to operate porous electrodes at the maximum rates everywhere within the bed. This is an ultimate goal in operating a flow-through porous electrode, fuel cell, or battery. At flow-through porous electrodes, maximum rates could be obtained if the polarization at the back of the porous electrode is large enough to support maximum currents without allowing the high polarization at the front of the electrode to stimulate a side reaction. In the present case, the problem is much more complicated as the hydrogen evolution reaction (HER) simultaneously occurs with the main reaction. This situation could occur when the main reaction has a more negative reversible potential than the HER (e.g., electrochemical deposition of nonnoble metals such as Zn or Cr). The HER is not mass-transfer controlled while the metal reaction is. In a previous model, the effects of different controlling groups and a simultaneous HER on the Coulombic efficiency of the metal reaction were simulated at flow-through porous electrodes.[1] Further efforts could still be undertaken to understand the behaviors of such systems. Flow-through porous electrodes have found different applications both in industrial and environmental applications.[2−6] They have the advantages of high specific surface area as well as high mass-transfer rates. However, porous electrodes frequently operate with nonuniform reaction rates, resulting in lower extents of utilization of the bed. It is therefore of crucial importance to estimate the fraction of the utilized surface area. The effectiveness factor has proved to be interesting in such aspects. The concept of the effectiveness factor has been introduced by a number of authors[7−10] for the analysis of the behavior of specific electrodes, but none have considered the combined ohmic and mass-transfer effects, bubble formation, and simultaneous reaction on the effectiveness factor.

The objective of the present study is to discuss the combined ohmic, kinetic, and mass-transfer effects along with bubble formation on the effectiveness factor of flow-through porous electrodes. The utilization extents at different conditions are discussed in light of a theoretical framework. The mathematical model is examined by comparing its theoretical predictions with the experimental results of zinc removal with simultaneous hydrogen evolution in a flow-through packed bed of zinc spheres.

Experimental Section

The working electrode was made of zinc spheres of 0.3 cm diameter. The packed-bed electrode had a specific surface area of 12 cm^{-1}, porosity of 0.50, diameter of 1.4 cm, thickness of 1.7 cm, and ohmic resistance of <0.01 ohm. The counter electrode was made of a platinum screen and was placed on the downstream side of the porous electrode (see Figure 1). The reference electrode was of the type Hg/HgO/1 M KOH. The potential reported here is that of the electrode relative to the downstream reference electrode (denoted as E). Current densities are reported on the basis of the geometrical cross-sectional area of the electrode (i.e., 1.54 cm^2). A potentiostat (EG&G model 273A) was used in all measurements. The cell voltage between the working electrode and the counter electrode was measured using a digital multimeter. The zincate solutions were prepared by dissolving the desired weights of ZnO in 3 M KOH. The solution was circulated using a variable speed pump, and the flow rate was measured using a floating-sphere-type flowmeter. The measurements were performed at 25 °C. Further details of the experimental part can be found elsewhere.[11]

* Present address: Karl-Winnacker-Institut der Dechema e.V.Theodor-heus-Alle 25D-6048 Frankfurt am Main, Germany. E-mail: mahmoudsaleh90@yahoo.com.

10.1021/jp048489w CCC: $27.50
Published on Web 08/05/2004

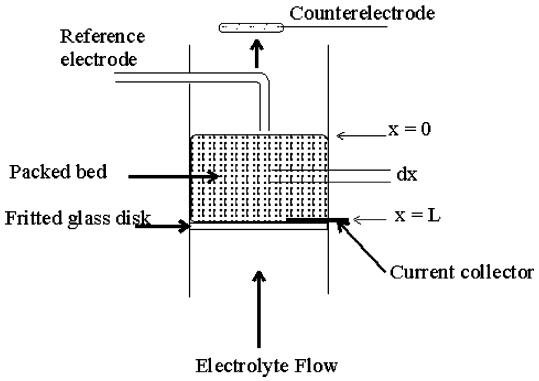

Figure 1. Schematic diagram of the porous electrode arrangement and flow direction.

Mathematical Model

The model equations have been developed to simulate the following simultaneous electrochemical reactions

$$M^{+n} + ne^- = M \quad E_M^\circ \tag{1}$$

$$2H^+ + 2e^- = H_2 \quad E_H^\circ \tag{2}$$

where M is an active metal (e.g., Zn or Cr) and $E_M^\circ < E_H^\circ$.

Figure 1 shows the arrangement of the porous electrode and the direction of the electrolyte flow. The model was developed under certain conditions. The Butler−Volmer equation governs the kinetic rates of both the metal and the hydrogen reactions but with a two- or one-electron charge-transfer rate-determining step, respectively. Conversion efficiency per single pass is low because we are suggesting higher flow rates to weep out the gas bubbles resulting from the HER. The solid matrix has uniform porosity and conductivity. Also, the effects of the double layer and the migration effects are negligible. The packed-bed electrode is characterized by a porosity of 0.7.

Butler−Volmer expressions for the metal and hydrogen reactions are given by eqs 3 and 4, respectively

$$\frac{di_M(x)}{dx} = -J_M(x) = \frac{-i_{o,M}S[1 - \exp(2\eta_M(x)/b)]}{\exp(\beta\eta_M(x)/b) + \frac{i_o}{i_L}} \tag{3}$$

$$\frac{di_H(x)}{dx} = -J_H(x) = \frac{-i_{o,H}S[1 - \exp((\eta_M(x) + \Delta E)/b)]}{\exp[\alpha(\eta_M(x) + \Delta E)/b]} \tag{4}$$

where $\Delta E = E_{rev,M} - E_{rev,H}$ and in the model calculations, it was taken as the difference in the standard reversible potentials such that $\Delta E = E_M^\circ - E_H^\circ$. An arbitrary difference value of −0.25 V was used here for the model calculations. J is the reaction current per unit volume of the porous matrix, and i is the solution current per unit of geometrical area. The rest of the symbols are found in the notation section. Note that $\eta_M(x) + \Delta E$ replaces $\eta_H(x)$ in eq 4. The local limiting current density of the metal reaction, i_L, is related to the local mass-transfer coefficient, k_m, and the bulk metal ion concentration, C, by

$$i_L = nFk_mC \tag{5}$$

The sum of the metal solution current and the hydrogen solution current is given by the total solution current, i

$$i(x) = i_M(x) + i_H(x) \tag{6}$$

Ohm's law governs the relationship between the total solution current traveling within the pore electrolyte and the polarization gradient, such that

$$i(x) = \kappa(x)\frac{d\eta_M(x)}{dx} \tag{7}$$

where $\kappa(x)$ is the pore electrolyte conductivity at a distance x. $\kappa(x)$ is given here by Brugmann's equation[12]

$$\kappa(x) = \kappa^\circ[\theta - \epsilon(x)]^{3/2} \tag{8}$$

where κ° is the conductivity of the bulk solution, and $\epsilon(x)$ is the gas void fraction. The latter, $\epsilon(x)$, is related to the hydrogen current, i_H, that produces it[12]

$$\epsilon(x) = \frac{\theta i_H(x)}{v\gamma + i_H(x)} \tag{9}$$

where γ is a conversion factor that converts coulombs passed to a volume of hydrogen gas, is given by

$$\gamma = \frac{2PF}{RT} \tag{10}$$

and equals 7.87 C cm^{-3} of hydrogen gas at standard temperature and pressure.[12] To obtain a system of equations of general applicability and to reduce the number of parameters, the above variables in the system were normalized to give the following system of dimensionless equations:

$$\frac{d\bar{i}_M(y)}{dy} = -\bar{J}_M(y) = \frac{-I_o[1 - \exp(2\bar{\eta}_M(y))]}{\exp(\beta\bar{\eta}_M(y)) + \frac{I_{o,M}}{I_L}} \tag{11}$$

$$\frac{d\bar{i}_H(y)}{dy} = -\bar{J}_H(y) = \frac{-[1 - \exp(\bar{\eta}_M(y) + \Delta\bar{E})]}{\exp[\alpha(\bar{\eta}_M(y) + \Delta\bar{E})]} \tag{12}$$

$$\bar{i}(y) = \bar{i}_M(y) + \bar{i}_H(y) \tag{13}$$

$$\bar{i}(y) = \sigma\bar{\kappa}(y)\frac{d\bar{\eta}_M(y)}{dy} \tag{14}$$

$$\bar{\kappa}(y) = [\theta - \epsilon(y)]^{3/2} \tag{15}$$

$$\epsilon(y) = \frac{\theta\bar{i}_H(y)}{\Psi + \bar{i}_H(y)} \tag{16}$$

The normalization was performed with $y = x/L$, $\bar{i} = i/i_{o,H}SL$, $\bar{\eta} = \eta/b$, and $\bar{\kappa} = \kappa/\kappa^\circ$.

As a result of this normalization, a number of dimensionless and dimensional governing groups were released, as shown in Table 1. The different groups have the following significant parameters: $I_{o,M}$ is the total exchange current density of the metal reaction. Smaller values of $I_{o,M}$ correspond to significant charge-transfer (activation) control of the metal reaction. The theoretical total limiting current, I_L, reflects the mass-transfer resistance to the metal reaction. Lower values of I_L indicate limiting metal reaction current and that the reaction is mass-transfer controlled. The kinetic ratio, I_o, determines how fast the metal reaction goes with respect to the HER. Higher values of I_o mean a faster metal reaction. The conductivity group, σ, determines the extent of ohmic control on the total reaction. Higher values of σ mean that the reaction is more uniform within

TABLE 1: Dimensional and Dimensionless Controlling Groups

group	definition
$I_{o,M} = i_{o,M}SL$	total exchange current density of the metal reaction
$I_L = i_L SL$	theoretical total limiting current
$I_o = I_{o,M}/I_{o,H} = i_{o,M}SL/i_{o,H}SL$	dimensionless kinetic ratio
$\sigma = \kappa^o b/I_{o,H}{\cdot}L$	dimensionless conductivity group
$\psi = v\chi/I_{o,H}$	dimensionless bubble group
$\Delta\bar{E} = \bar{E}_{rev,M} - \bar{E}_{rev,H}$	dimensionless difference in reversible potentials
$\alpha = 0.5$	charge transfer coefficient of hydrogen reaction
$\beta = 1$	charge transfer coefficient of the metal reaction
θ	porosity

the bed. Finally, the bubble group, Ψ, accounts for the extent of bubble formation. Lower values of Ψ indicate higher extents of bubble formation.

Boundary conditions are as follows

$$y = 0 \quad \bar{i} = i_{cell}/I_{o,H}$$

$$y = 1 \quad \bar{i} = \bar{i}_M = \bar{i}_H = 0, \frac{d\bar{\eta}}{dy} = 0, \bar{\kappa} = \theta^{1.5}, \text{and } \epsilon = 0$$

The above system of equations was solved for the six unknowns, which are $\bar{\imath}$, $\bar{\eta}$, $\bar{\imath}_M$, $\bar{\imath}_H$, $\bar{k}$, and ϵ, by using a numerical technique developed by Newman.[13]

Theoretical Results and Discussion

The results of the theoretical model are presented here in order to investigate the different combined effects on the extent of utilization of the porous electrode by introducing the concept of the effectiveness factor, Φ, which is given in the present study by

$$\Phi = \frac{\text{total obtainable limiting current}}{\text{maximum limiting current}} \qquad (17)$$

The total obtainable limiting current could be obtained from the inflection in the polarization curves at a certain set of parameters. The maximum limiting current is obtained by the same procedure at the same set of parameters but at infinite value of the conductivity group, σ. Under the last condition, the dimensionless polarization of the metal reaction at the front face, $\bar{\eta}_M|_{y=0}$, equals the polarization at any distance y within the bed, and the limiting current is the maximum limiting current.

I. Negligible Bubble Formation. The combined effects of mass-transfer, kinetic, and ohmic resistance on the effectiveness factor are presented here. This could be simulated by solving the dimensionless model equations (eqs 11−16), putting Ψ as an infinite value. The $I_{o,M}$ value was used as 0.2 A cm^{-2} in all of the model calculations. Figures 2 and 3 show the effects of the conductivity group, σ, on metal polarization curves at values of the kinetic ratio, I_o, equal to 1×10^4 and 2×10^4, respectively. The polarization curves were constructed by plotting the dimensionless metal polarization, $\bar{\eta}_M|_{y=0}$, (at the front of the electrode) with the corresponding dimensionless metal solution current, $\bar{\imath}_M|_{y=0}$. Both figures are calculated at a value of the theoretical total limiting current, I_L, equal to 0.25 A cm^{-2}. The figures reveal current plateaus, their values depending on σ and I_o. As the conductivity group σ increases, the total obtainable limiting current increases (as indicated by

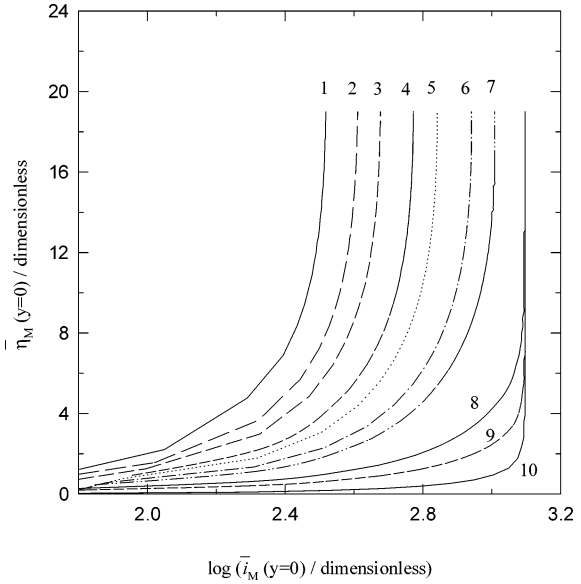

Figure 2. Polarization curves for the metal reaction at different conductivity groups, σ's. $I_L = 0.25$ A cm^{-2} and $I_o = 10^4$. Bubble effects are negligible. $\sigma = 12$ (1), 18 (2), 25 (3), 37 (4), 50 (5), 75 (6), 10^2 (7), 250 (8), 5×10^2 (9), and 1×10^3 (10).

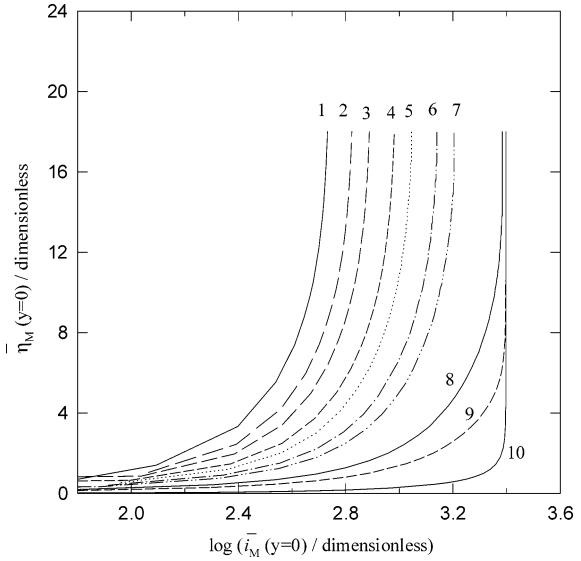

Figure 3. Polarization curves for the metal reaction at different conductivity groups, σ's. $I_L = 0.25$ A cm^{-2} and $I_o = 2 \times 10^4$. Bubble effects are negligible. $\sigma = 12$ (1), 18 (2), 25 (3), 37 (4), 50 (5), 75 (6), 10^2 (7), 250 (8), 5×10^2 (9), and 1×10^3 (10).

the shift of the plateau to larger limiting current values) until it reaches a constant value independent of σ. In Figure 2, for instance, no more shifts of the limiting currents are found for $\sigma = 2.5 \times 10^2$, 5×10^2, and 1×10^3 (lines 8, 9, and 10, respectively). As will be shown in Figure 6, at $\sigma = 1 \times 10^3$, the metal polarization is uniform everywhere within the bed, and consequently, the metal reaction is fully uniform. Hence, the obtainable total limiting current in this case (at $\sigma = 1 \times 10^3$) is the maximum total limiting current. This value is what had been used in eq 17 to calculate the effectiveness factor, Φ, at different σ. A similar strategy was followed to obtain the maximum total limiting currents at different conditions. The data were analyzed by extracting the values of the total obtainable limiting current at an arbitrary value of the dimensionless polarization of 14. Using the extracted values of the obtainable total limiting currents at different conditions allowed us to calculate the effectiveness factor using eq 17. Similar pairs

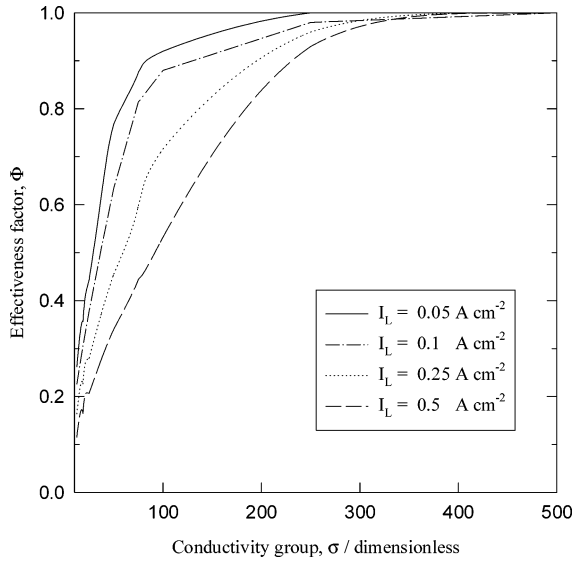

Figure 4. Effects of the conductivity group, σ, on the effectiveness factor at different values of the theoretical total limiting current, I_L and $I_o = 10^4$. Bubble effects are negligible.

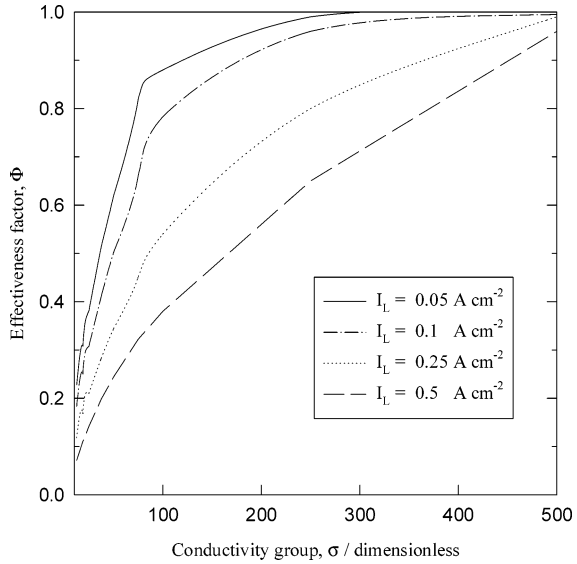

Figure 5. Effects of the conductivity group, σ, on the effectiveness factor at different values of the theoretical total limiting current, I_L and $I_o = 2 \times 10^4$. Bubble effects are negligible.

of the above polarization curves (Figures 2 and 3) were collected at different values of I_L, mainly at $I_L = 0.05$, 0.1, and 0.5 A cm^{-2}. At each value of I_L, the polarizations curves were obtained in pairs at the above two values of the kinetic ratio, I_o, mainly 1×10^4 and 2×10^4.

Figures 4 and 5 show the effects of the conductivity group, σ, on the effectiveness factor, Φ, at different values of the theoretical total limiting current, I_L. The two figures were obtained from the analysis of Figures 2 and 3 and the other similar figures as discussed above. The values of I_o used in Figures 4 and 5 were 1×10^4 and 2×10^4, respectively. The rest of the parameters used to construct Figures 4 and 5 are the same as those used in Figures 2 and 3, respectively. For certain values of I_L and I_o, the effectiveness factor increases with σ until it reaches a constant maximum value of 1. At lower values of σ ($\sigma < 30$), Φ has lower sensitivity to the change in I_L than at higher values of σ (i.e., $\sigma > 30$). At lower values of σ, the reaction is ohmic-controlled and pushed to a thin layer at the front of the porous electrode, leading to high localization of the reaction current. At higher values of σ, the polarization becomes more uniform and can support limiting currents both at the front and, to different extents, at the back of the electrode (see discussion of Figures 6 and 7). As the conductivity group increases, the potential becomes more uniform, and hence, the current becomes more uniform, resulting in more extensive utilization of the bed. This is in accordance with Ohm's Law. On the other hand, I_L has a significant effect on Φ. At a certain value of σ, the effectiveness factor increases as I_L decreases. At lower values of I_L (e.g., $I_L = 0.05$ A cm^{-2}), we reached $\Phi = 1$ at $\sigma \approx 200$, whereas at $I_L = 0.5$ A cm^{-2}, a value of $\Phi = 1$ was delayed until a larger value of σ was reached (i.e., at $\sigma \approx 400$). In other words, the increase of I_L retards higher extents of utilization of the porous bed, and 100% utilization required higher values of the conductivity group. Higher polarizations at the exit face can support only higher limiting currents, while at the back of the electrode, lower polarization supports only lower currents. The system is now under mixed mass-transfer and ohmic control. In the case of lower values of I_L, the reaction could be supported by both the high polarization at the exit face and the lower polarization at the back of the electrode. At lower I_L values, the metal reaction is mass-transfer limited everywhere within the bed, and a minimum conductivity group could cause uniform current distributions. Lower polarizations could support limiting currents everywhere within the bed. The figures also reveal the effects of the kinetic ratio, I_o, on Φ. The effectiveness factor increases with the decrease of I_o. The effects of I_L on Φ are more pronounced at higher I_o, as seen in Figure 5. To obtain higher values of Φ at higher I_o (higher reaction rates), the values of σ should be increased. For instance, a value of $\Phi = 1$ is reached at $I_L = 0.5$ and at $I_o = 1 \times 10^4$ when $\sigma = 400$ (Figure 4). However, when I_o is doubled to 2×10^4 (Figure 5), a value of $\sigma > 500$ is required to obtain the same $\Phi = 1$ at the same I_L. The discussions here conclude that the improvement of Φ values at higher I_L and/or I_o (i.e., at higher rates) could be obtained by using higher values of σ. The conductivity group σ increases as the conductivity of the electrolyte κ° increases, the total exchange current density of the HER ($I_{o,H}$) decreases, and/or the electrode thickness L decreases (see Table 1). Because σ depends on structure, transport, and kinetic parameters, this could help to guide the design of the porous electrode.

Study of the reaction current distributions of the metal reaction at different conditions could help to understand the effects of different groups on Φ. Figure 6 shows the distributions of the dimensionless metal polarization at different values of σ at $I_L = 0.1$ A cm^{-2} and $I_o = 2 \times 10^4$. As the conductivity group σ increases, the polarization becomes more uniform, and virtually at $\sigma = 5 \times 10^2$, the polarization at the front of the electrode equals the polarization everywhere within the bed. Under these conditions, full utilization of the bed is obtained, and the total limiting current is maximum under the present set of conditions. Lower extents of utilization are obtained as σ decreases. Consequently, the reaction current distributions of the metal reaction are affected. This is shown in Figure 7, which was calculated at the same conditions as Figure 6. As σ increases, the reaction becomes more uniform. A full utilization of the bed could be obtained at a value of $\sigma = 5 \times 10^2$, and hence, a value of $\Phi = 1$ is obtained. However, lower values of Φ were obtained at lower values of σ. Apparent values of Φ at different values of σ, as estimated from current distributions of Figure 7 (from areas under the curves), are comparable with those obtained in Figure 5 at the same conditions.

Figure 8 shows the current distributions of the metal reaction at different values of I_L. As I_L increases, the reaction current becomes more nonuniform. At lower limiting current, the reaction is mass-transfer limited everywhere within the porous

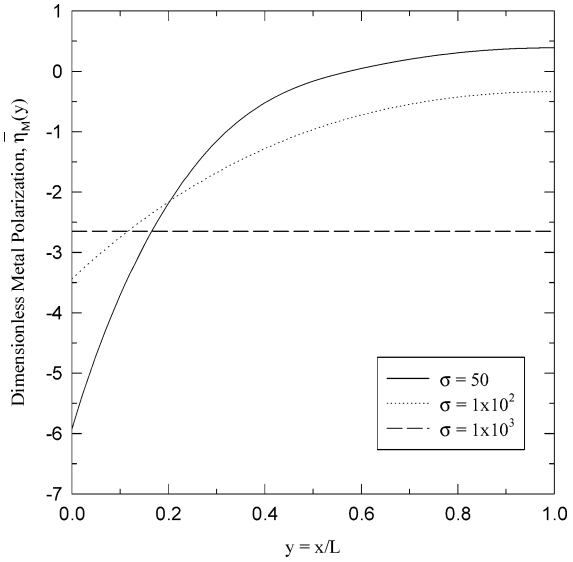

Figure 6. Effects of σ on the distribution of the dimensionless polarization of the metal reaction at $I_L = 0.1$ A cm^{-2} and $I_o = 2 \times 10^4$.

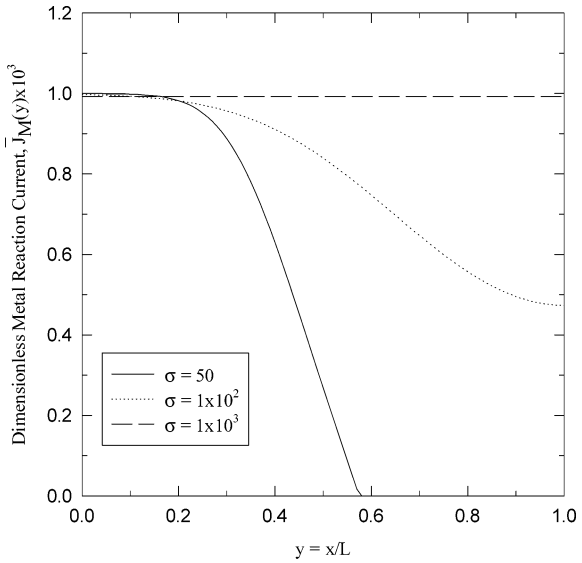

Figure 7. Effects of σ on the distribution of the dimensionless reaction current of the metal reaction at $I_L = 0.1$ A cm^{-2} and $I_o = 2 \times 10^4$.

bed, and a limiting current condition could be obtained throughout the whole bed. However, at high I_L, the reaction is only limited at the front of the electrode but suffers lower currents at the back of the electrode. This is because high polarization at the front of the electrode can support higher limiting currents, but at the back of the electrode, lower polarization can only support currents that are much lower than the limiting currents.

II. Appreciable Bubble Formation. Because the competitive reaction here is a hydrogen evolution reaction, it is reasonable to account for the effects of the gas bubble formation on the effectiveness factor. The generated gas bubbles decrease the cross-section available for ionic flow and, consequently, decrease the effective conductivity of the pore electrolyte (see eq 8). Studying the effects of bubble formation on the effectiveness factor of the porous electrode implied that eqs 11−16 were solved simultaneously, taking into account the bubble group, Ψ, which expresses the extent of bubble formation.

Figure 9 shows the effects of the bubble group, Ψ, on the distributions of both the gas void fraction, $\epsilon(y)$ (- - -) and the

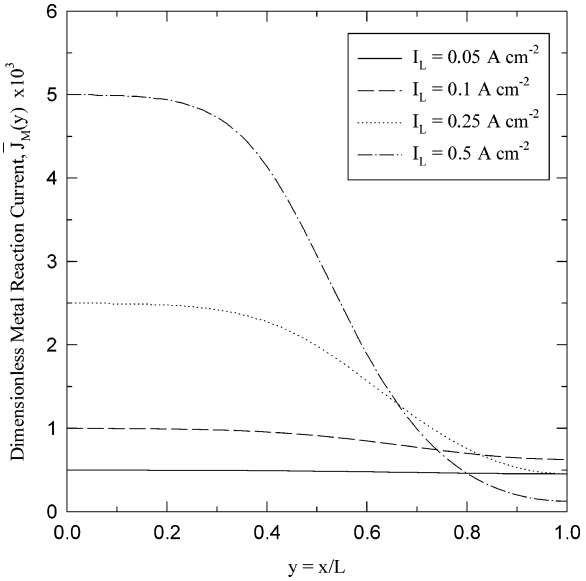

Figure 8. Effects of I_L on the distributions of the dimensionless metal reaction current at $\sigma = 250$ and $I_o = 2 \times 10^4$.

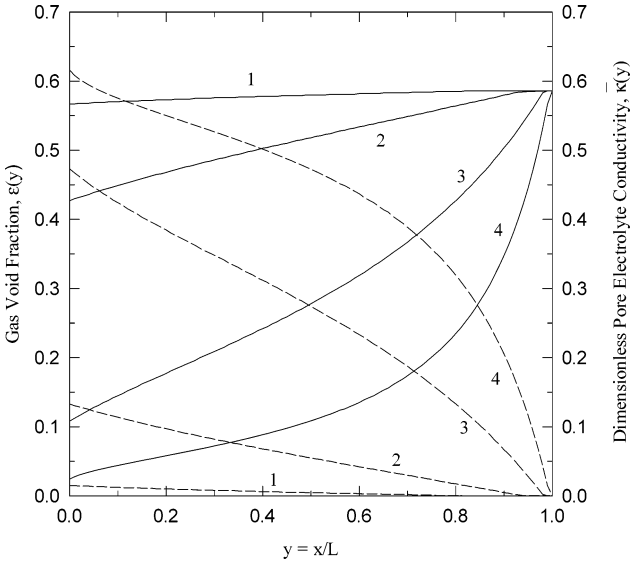

Figure 9. Effects of the bubble group, Ψ, on the distributions of the gas void fraction and the dimensionless pore electrolyte conductivity. $I_L = 0.1$ A cm^{-2}, $I_o = 1 \times 10^4$, and $\sigma = 250$. $\Psi = 30$ (1), 5 (2). 1 (3), 0.25 (4) (all Ψ values are $\times 10^3$).

dimensionless pore electrolyte conductivity, $\bar{\kappa}(y)$ (—). Generally, as Ψ decreases, the gas void fraction increases and the amount of bubbles filling the pore electrolyte increases. For instance, at a value of $\Psi = 2.5 \times 10^2$ (Figure 9, line 4), more than 50% of the porous bed is plugged with gas bubbles. As Ψ increases, the gas void fraction decreases, and at a value of $\Psi = 3 \times 10^4$ (Figure 9, line 1), no significant bubble formation is observed. Note that higher values of Ψ mean higher values of the flow rate, v, and/or lower values of the total exchange current density of the hydrogen reaction, $I_{o,H}$. The figure reveals also that, at $\Psi = 3 \times 10^4$, the dimensionless pore electrolyte conductivity, $\bar{\kappa}(y)$, equals nearly a constant value, which equals $\theta^{1.5}$, indicating negligible bubble formation (see eq 15). At lower values of Ψ (higher extents of bubble formation), $\bar{\kappa}(y)$ has lower values. As $\bar{\kappa}(y)$ increases, the polarization of the metal reaction becomes more nonuniform.

Polarization curves similar to those presented in Figures 2 and 3 were collected at different values of the bubble group, Ψ, at the same conditions mentioned in the discussion of Figure

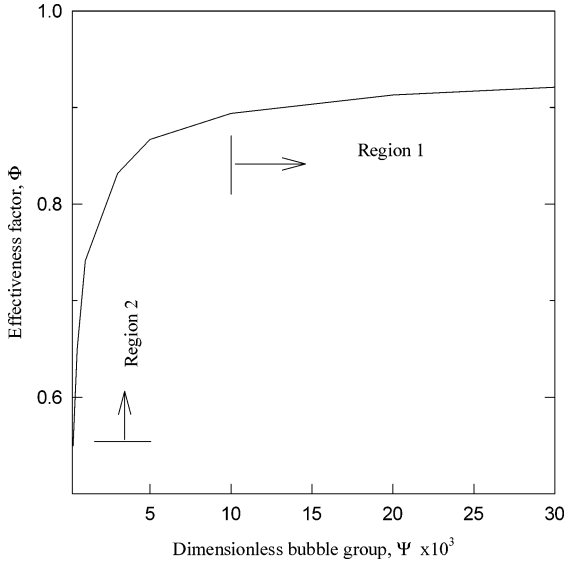

Figure 10. Effects of the bubble group, Ψ, on the effectiveness factor. $I_L = 0.1$ A cm^{-2}, $I_o = 1 \times 10^4$, and $\sigma = 250$. Regions 1 and 2 correspond to negligible and significant bubble formation, respectively.

9. Similar analysis was performed here for the polarization curves to calculate the effectiveness factor at different values of Ψ. Figure 10 shows the effects of the bubble group, Ψ, on the effectiveness factor at $I_L = 0.1$ A cm^{-2}, $I_o = 1 \times 10^4$, and $\sigma = 2 \times 10^2$. As Ψ increases, the effectiveness factor increases until it reaches a constant value. At lower values of Ψ (Ψ < 1×10^4), and as seen in region 2 in Figure 10, the bubble formation is significant, and the pore electrolyte conductivity has lower values resulting in more nonuniform distributions of the potential and, consequently, more nonuniform distributions of the metal reaction current. The reaction in this case is restricted to a thinner layer at the front of the electrode. Therefore, lower utilizations of the bed were obtained, and Φ decreases. The bubble formation accentuates the ohmic effects. As Ψ increases, the extent of bubble formation decreases until it becomes negligible at Ψ > 1.5×10^4 (region 1 in Figure 10), and hence, Φ reaches a high constant value. This constant value could be compared with the value obtained in Figure 4 at the same values of the parameters used when the gas bubble formation was neglected (see section I, Negligible Bubble Formation).

Test of the Model Predictions

In this section, the model is tested by fitting the experimental data with the model predictions under selected experimental conditions. The electrochemical removal of zinc from alkaline zincate solution was used as an example. It involves two simultaneous reactions:

$$Zn(OH)_4^{2-} + 2e^- = Zn + 4OH^- \quad E^\circ_{Zn} = -1.29 \text{ V (SHE)} \tag{18}$$

$$2H_2O + 2e^- = H_2 + 2OH^- \quad E^\circ_{H} = -0.83 \text{ V (SHE)} \tag{19}$$

The extent of competition of the hydrogen reaction depends on the kinetic, thermodynamic, mass-transfer, and ohmic resistances. The effects of the electrolyte flow rate, v, on the present system are tested here. The increase of v enhances the mass-transfer rate leading to higher limiting currents of the metal reaction. Moreover, it helps to sweep the gas bubbles out of the porous matrix resulting in a decrease of the gas void fraction.

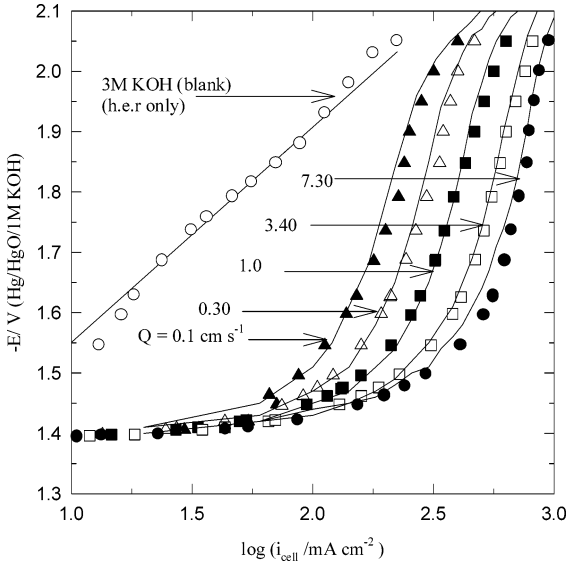

Figure 11. Effects of the electrolyte flow rate, v, on the total current−potential relations of zinc deposition from 0.08 M zincate solution in 3 M KOH. Symbols are the experimental data, and lines are the model predictions.

TABLE 2: Fitting Parameters

parameter	fitting value	literature value	ref
$i_{o,Zn}$	6.0×10^{-2} A cm^{-2}	same value	14
$i_{o,H}$	2.0×10^{-9} A cm^{-2} [a]	1.0×10^{-9} A cm^{-2}	15
D	1.5×10^{-5} cm^2 s^{-1}	6.0×10^{-6} cm^2 s^{-1}	16
ν	0.01 g cm^2 s^{-1}	same value	17
κ^o	0.4 ohm^{-1} cm^{-1}	same value	18
α	0.4	accepted value 0.5	15
β	1.0	same value	14

[a] This value was obtained by fitting the polarization curve for the hydrogen evolution reaction (the blank 3 M KOH curve in Figure 11) with the model prediction in the absence of the zinc reaction.

Figure 11 shows the effects of the electrolyte flow rate, v, on the $i-E$ relationship for zinc deposition from alkaline zincate solution of concentration equal to 0.08 M ZnO in 3 M KOH. The figure also shows the $i-E$ relationship for HER from 3 M KOH (blank). The symbols show the experimental data while the lines are the model predictions. Note that i_{cell} shown in the figure refers to the total solution current at the front of the electrode, where $i_{cell} = i_{Zn}|_{x=0} + i_H|_{x=0}$, which corresponds to a potential $E = \eta_{Zn}|_{x=0} + E_{rev}(Zn)$. The fitting parameters used to perform the model calculations are listed in Table 2. The local mass-transfer coefficient was taken from empirical correlations[19]

$$k_m = 1.17 v^{0.58} \left[\frac{d}{\nu}\right]^{-0.42} \left[\frac{\nu}{D}\right]^{-0.67} \tag{20}$$

The equilibrium potentials of both the zinc and hydrogen reactions were taken, respectively, as

$$E_{rev,Zn} = A_0 + A_1 \log M[OH^-] + A_2 \log M[Zn(OH)_4^{2-}] \tag{21}$$

$$E_{rev,H} = \frac{-2.303RT}{F} \text{pH} \tag{22}$$

where the A's are constants depending on temperature, and M[KOH] and M[Zn(OH)$^{-4}$] are the molarities of the hydroxide and zincate ions, respectively.[20] On solving the dimensional model (eqs 3, 4, 6−9), ΔE in eq 4 was taken as $E_{rev,Zn} - E_{rev,H}$. Figure 11 reveals satisfactory agreement between the model

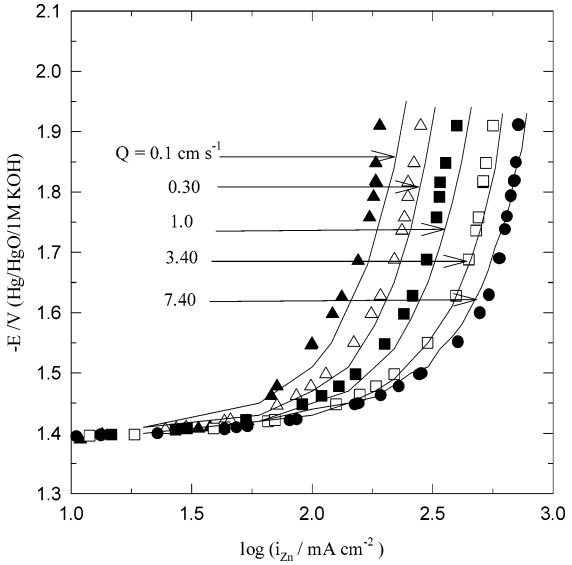

Figure 12. Effects of the electrolyte flow rate, v, on the (zinc current) $i_{Zn}-E$ relations of the zinc reaction from 0.08 M zincate solution in 3 M KOH. Symbols are the experimental data, and lines are the model predictions.

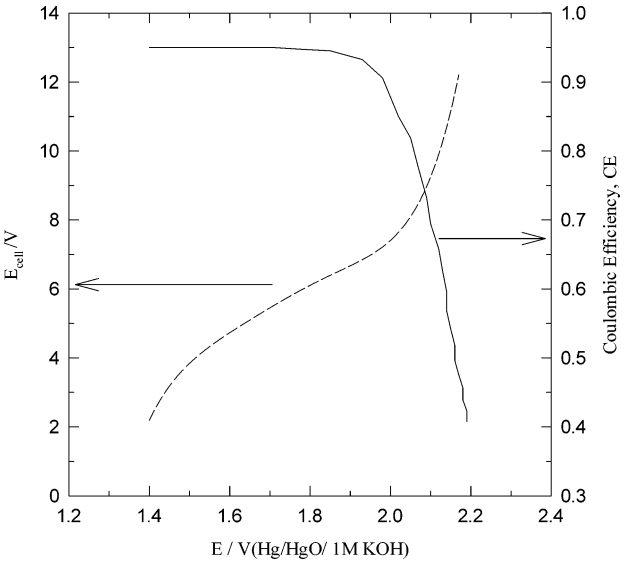

Figure 13. Changes of the Coulombic efficiency and the cell voltage with the electrode potential at $v = 1.0$ cm s^{-1} and other parameters as in Figure 12.

predictions and the experimental data. The polarization curves show broad limiting currents.

Sharper limiting currents were obtained by subtracting the hydrogen current, $i_H|_{x=0}$ (of the hydrogen curve) from the total cell current to obtain the zinc current, $i_Z|_{x=0}$. This is discussed in Figure 12 which shows polarization curves only for the zinc reaction at different electrolyte flow rates at the same parameters used in Figure 11. The total limiting currents either from experimental data or model predictions were estimated at the inflections in the polarization curves of the zinc reaction shown in Figure 12 at an arbitrary potential of ~ -1.85 V. The choice of this arbitrary potential can be explained from the following discussion. Figure 13 shows plots of the cell voltage, E_{cell}, with the electrode potential, E (left y-axis), and the Coulombic efficiency, CE, with the electrode potential, E (right y-axis), under the same conditions as those in Figure 11. One flow rate of 1.0 cm s^{-1} was used in Figure 12. The Coulombic efficiency, CE, of the zinc reaction was taken as $i_{Zn}|_{x=0}$ /i_{cell}. As the electrode potential increases, the Coulombic efficiency, after

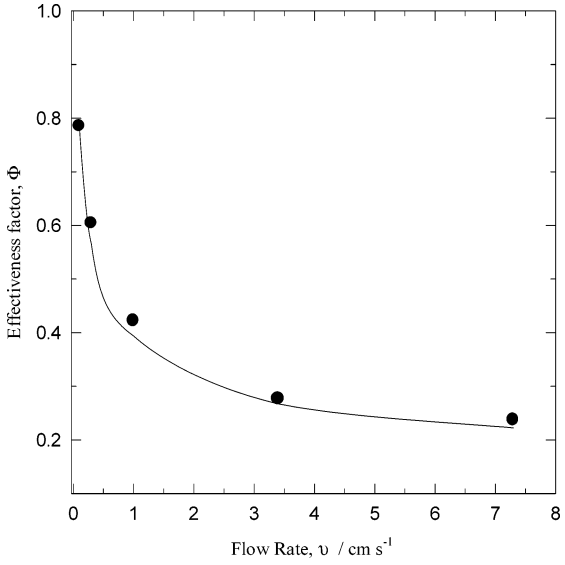

Figure 14. Effects of the flow rate, v, on the effectiveness factor at the experimental conditions used in Figure 11. Symbols are the experimental data, and the line is the model prediction.

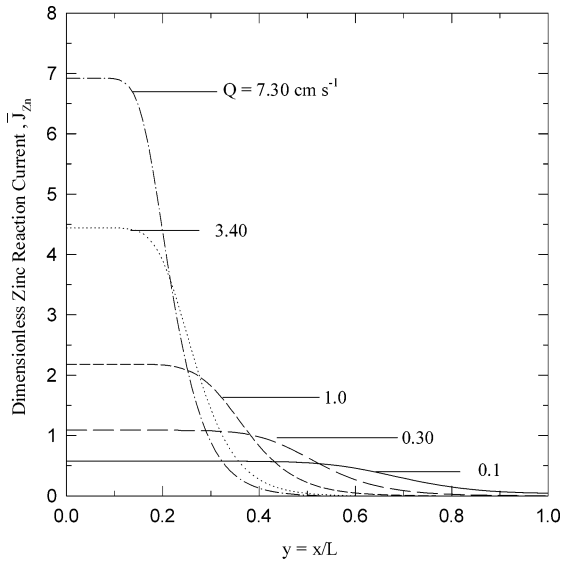

Figure 15. Distributions of the dimensionless zinc reaction current at different values of the flow rate, v.

passing through a plateau, decreases sharply at a potential of ~ -1.85 V (Hg/HgO/1 M KOH). Also, at this electrode potential, the cell voltage begins to increase dramatically (exponentially). This supports the fact that the chosen arbitrary potential is reasonable under the present operating parameters. Other flow rates showed similar arbitrary potential.

The estimated values of the limiting currents at different flow rates were used to calculate the effectiveness factor, Φ, at different flow rates. These values represent the total obtainable limiting current. To calculate the effectiveness factor, the maximum total limiting current should be determined (recall eq 17). Because the dimensional model is used in this section, the theoretical total limiting current (i.e., $I_L = i_L SL$) was taken as the maximum total limiting current. From its definition, it is the total limiting current when the reaction is fully uniform, that is, the porous electrode works as a planar electrode with high surface area.[12] If we combined eqs 5 and 20 and used the system parameters shown in Table 1, I_L could be calculated at different values of v. For instance, $I_L = 1.10 \times v^{0.58}$. Figure 14 shows plots of the effectiveness factor Φ against v. The line shows the model predictions, and the symbols show the

experimental values. Satisfactory agreements between the model predictions and the experimental data are revealed in Figure 14. As the flow rate increases, the effectiveness factor decreases, in the beginning to a greater extent until $v = 1.0$ cm s^{-1} and then to a lesser extent at $v > 1.0$ cm s^{-1}. Note that v has a net effect on both the total limiting current and the bubble group. At lower flow rates, the limiting currents are low, the metal reaction is limited everywhere within the bed, and lower polarizations could support lower limiting currents. Hence, the metal reaction is more uniform throughout the bed. At higher v (i.e., high limiting currents), the reaction is limiting only at the front of the electrode where higher polarizations could support higher limiting currents, while the back of the electrode suffers from lower currents. In this case, greater utilization of the porous bed could be obtained at lower flow rates. This is in agreement with the theoretical results shown for the effects of I_L on Φ, as depicted earlier in Figures 4 and 5.

To further illustrate this result, it is reasonable to study the current distributions of the zinc reaction at the estimated total limiting current values used in Figure 14. Figure 15 shows such distributions at different corresponding limiting currents. As v increases (i.e., total limiting current increases), the distributions of the metal reaction current become more nonuniform. Greater utilization of the bed thickness was obtained at lower flow rates. These results support the conclusions derived in Figure 14.

Summary and Conclusions

This study was devoted to investigating the effects of different combined effects on the extent of utilization of a flow-through porous electrode operating for simultaneous reactions. The utilization extent was defined as an effectiveness factor, Φ. Those effects included mass-transfer, ohmic, kinetic, and bubble formation. By using a mathematical model, it was feasible to introduce a number of controlling groups. The increases in I_L and/or I_o decrease Φ, resulting in possible local plugging of the porous matrix. In this case, higher values of σ were required to reach reasonably high values of Φ. The increase in both σ and Ψ causes an increase of Φ. The unavoidable side reaction restricted higher utilization extents of the porous electrode. A satisfactory agreement between the model predictions and the experimental data was obtained.

List of Symbols

$b = RT/F$, V

C = metal ion concentration in the bulk solution, g mol/cm^3

CE = Coulombic efficiency

d = diameter of the packed-bed particle, cm

D = diffusion coefficient, cm^2 s^{-1}

E_{rev} = reversible potential of the electrochemical reaction, V

ΔE = difference in reversible potential between metal and hydrogen reactions, V

F = Faraday's constant, 96 500 C equiv^{-1}

$i(x)$ = total solution current per unit cross-sectional area of the packed bed, A cm^{-2}

i_{cell} = applied cell current per unit cross-sectional area of the packed bed, A cm^{-2}

I_L = theoretical total limiting current supported by the packed bed, $i_L SL$

i_L = metal limiting reaction current per unit reaction area, A cm^{-2}, eq 5

$i_M(x)$ = local metal solution current per unit cross sectional area, A cm^{-2}

$i_H(x)$ = local hydrogen solution current per unit cross sectional area, A cm^{-2}

I_o = kinetic ratio = $i_{o,M}SL/i_{o,H}SL$

$I_{o,M}$ = total exchange current density of the metal reaction, $i_{o,M}SL$

$I_{o,H}$ = total exchange current density of the hydrogen reaction, $i_{o,H}SL$

i_o = exchange current density based on the reaction area, A cm^{-2}

$J(x)$ = local reaction current per unit volume of the packed bed, A cm^{-3}

$\bar{J}(y)$ = dimensionless local reaction current, $J(x)/(I_{o,H}/L)$

k_m = local mass-transfer coefficient, cm s^{-1}

σ = dimensionless conductivity group, Table 1

L = electrode thickness, cm

P = pressure, atm

v = electrolyte flow velocity, cm s^{-1}

R = gas constant, 82.06 (cm^3·atm)/(mol·K)

S = specific surface area, cm^{-1}

T = absolute temperature, K

x = distance within the electrode, cm

y = dimensionless distance within the electrode

α = charge-transfer coefficient of the hydrogen evolution reaction (HER)

β = charge-transfer coefficient of the metal reduction

γ = constant = $2PF/RT$, C cm^{-3}

$\epsilon(x)$ = gas void fraction of the pore volume, dimensionless, eq 8

$\kappa(x)$ = pore electrolyte conductivity, ohm^{-1} cm^{-1}, eq 7

$\bar{\kappa}(y)$ = pore electrolyte conductivity, dimensionless, eq 15

κ° = conductivity of the bulk electrolyte, ohm^{-1} cm^{-1}

Ψ = dimensionless bubble group $v\gamma/I_{o,H}$

η_M = metal reaction overpotential, V

η_H = hydrogen evolution reaction (HER) overpotential, V

Φ = effectiveness factor, dimensionless.

θ = porosity

ν = kinematic viscosity, g cm^2 s^{-1}

References and Notes

(1) Saleh, M. M.; Weidner, J. W.; Ateya, B. G. *J. Electrochem. Soc.* **1995**, *142*, 4113.

(2) Friedrich, J. M.; Ponce-de-Leon, C. G.; Reads, W.; Walsh, F. C. *J. Electroanal. Chem.* **2004**, *561*, 203.

(3) Lanza, M. R. V.; Bertazzoli, R. *J. Appl. Electrochem.* **2000**, *30*, 61.

(4) Coeuret, F.; Oliveira, V. E.; Bezerra, C. E. *J. Appl. Electrochem.* **2002**, *32*, 1175.

(5) Newman, J.; Tiedman, W. *Advances in Electrochemistry and Electrochemical Engineering*; Gerischer, H., Tobias, C. W., Eds.; Wiley: New York, 1978; Vol. 11, p 352.

(6) Sioda, R. E.; Keating, K. B. *Electroanalytical Chemistry*; Bard, A. J., Ed.; Marcel Dekker, Inc.: New York, 1982; Vol. 12.

(7) Boyer, C. C.; Anthony, R. G. *J. Appl. Electrochem.* **2000**, *30*, 777.

(8) Goodridge, F.; Hamilton, M. A. *Electrochim. Acta* **1980**, *25*, 481.

(9) Scott, K. *Electrochim. Acta* **1983**, *28*, 1191.

(10) Kreysa, G. *Electrochim. Acta* **1978**, *23*, 1351.

(11) El-Deab, M. S.; Saleh, M. M.; El-Anadouli, B. E.; Ateya, B. G. *J. Electrochem. Soc.* **1999**, *146*, 208.

(12) Saleh, M. M. *Electrochim. Acta* **1999**, *45*, 959.

(13) Newman, J. *Electrochemical Systems*, 2nd ed.; Prentice-Hall: Englewood Cliffs, NJ, 1991; p 552.

(14) Bockris, J. O.; Nagy, Z.; Damjanovic, A. *J. Electrochem. Soc.* **1972**, *119*, 285.

(15) Lee, T. S. *J. Electrochem. Soc*. **1971**, *118*, 1278.

(16) Naybour, R. D. *Electrochim. Acta* **1968**, *13*, 763.

(17) St-pierre, J.; Piron, D. L. *J. Electrochem. Soc*. **1992**, *139*, 105.

(18) Dobos, D. *Electrochemical Data*; Elsevier Scientific Publishing Company: Amsterdam, 1975; pp 242 and 267.

(19) Cussler, L. E. *Diffusion and Mass Transfer*; Cambridge University Press: Cambridge, MA 1984; p 230.

(20) Isaacson, M. G.; McLarnon, F. R.; Carins, E. J. *J. Electrochem. Soc*. **1990**, *137*, 2361.